# Supplementary Information

## In silico design and experimental validation of a high-entropy perovskite oxide for SOFC cathodes

Jyotsana Kala,[a,b] Vicky Dhongde,[a,c] Subhrajyoti Ghosh,[a,c] Madhulika Gupta,*[d] Suddhasatwa Basu,[c] Brajesh Kumar Mani,*[b] M. Ali Haider*[a,e]

[a] Renewable Energy and Chemicals Lab, Department of Chemical Engineering, Indian Institute of Technology Delhi, Hauz Khas, New Delhi-110016, Delhi, India

[b]Computational Many Body Physics Lab, Department of Physics, Indian Institute of Technology Delhi, Hauz Khas, New Delhi-110016, Delhi, India

[c]Fuel Cell Lab, Department of Chemical Engineering, Indian Institute of Technology Delhi, Hauz Khas, New Delhi-110016, Delhi, India

[d]Computational Biophysics Lab, Department of Chemistry and Chemical Biology, Indian Institute of Technology (Indian School of Mines), Dhanbad-826004, Jharkhand, India

[e]Indian Institute of Technology (IIT) Delhi - Abu Dhabi, Khalifa City B, Abu Dhabi, United Arab Emirates

**Email:** madhulikagupta@iitism.ac.in, bkmani@physics.iitd.ac.in, haider@iitd.ac.in

## 1. Force-field parameters for molecular dynamics simulations

The Buckingham pairwise potential parameters used in MD simulations for cations and oxygen interactions are shown below in Table S1.

**Table S1** The Buckingham pairwise potential parameters for cation and oxygen anion interaction.

| **Ion Pair** | $A_{ij}$ **(eV)** | $\rho_{ij}$ **(Å)** | $C_{ij}$ **(eV Å$^6$)** |
|---|---|---|---|
| $La^{+3}$-$O^{-2}$ [Ref.[1]] | 1928.62 | 0.3321 | 0.00 |
| $Pr^{+3}$-$O^{-2}$ [Ref.[2]] | 1445.20 | 0.3608 | 0.00 |
| $Nd^{+3}$-$O^{-2}$ [Ref.[3]] | 2686.60 | 0.3206 | 0.00 |
| $Gd^{+3}$-$O^{-2}$ [Ref.[4]] | 1458.38 | 0.3522 | 0.00 |
| $Ba^{+2}$-$O^{-2}$ [Ref.[5]] | 1214.40 | 0.3522 | 0.00 |
| $Sr^{+2}$-$O^{-2}$ [Ref.[6]] | 959.10 | 0.3721 | 0.00 |
| $Ca^{+2}$-$O^{-2}$ [Ref.[7]] | 1227.70 | 0.3372 | 0.00 |
| $Mn^{+3}$-$O^{-2}$ [Ref.[8]] | 8474.57 | 0.2392 | 0.00 |
| $O^{-2}$-$O^{-2}$ [Ref.[9–11]] | 22764.3 | 0.1490 | 43.00 |

## 2. Input crystal structure information

The input LMO structure is derived from a prior experimental study, and subsequent optimization was performed using DFT simulations. Similarly, parent Sr-doped LSM20 and LSM50 structures from prior experimental studies are considered and subsequently optimized using DFT. In the case of high entropy structures, the LMO structure is extended to a 5×2×1 supercell. A-site is doped with five different cations to create LSBNP and LSCGP high entropy perovskite oxide. In order to generate randomness at the A-site, the mcsqs[12] code of ATAT[13–15] is used. A-site randomly doped structures are optimized in DFT in three steps. In the first step, only the atomic positions of the atoms are relaxed without relaxing the lattice parameters using the ISIF = 2 tag of VASP[16]. In the next step, both atomic positions and lattice parameters are optimized by

keeping the volume of the cell fixed using the ISIF = 4 tag of VASP[16]. In the last step, both lattice parameters and atomic positions are fully relaxed with changes in volume using the ISIF = 3 tag of VASP[16]. Table S2 and Figure S1 represent the input crystal structure information of parent perovskite oxides and high entropy perovskite oxides.

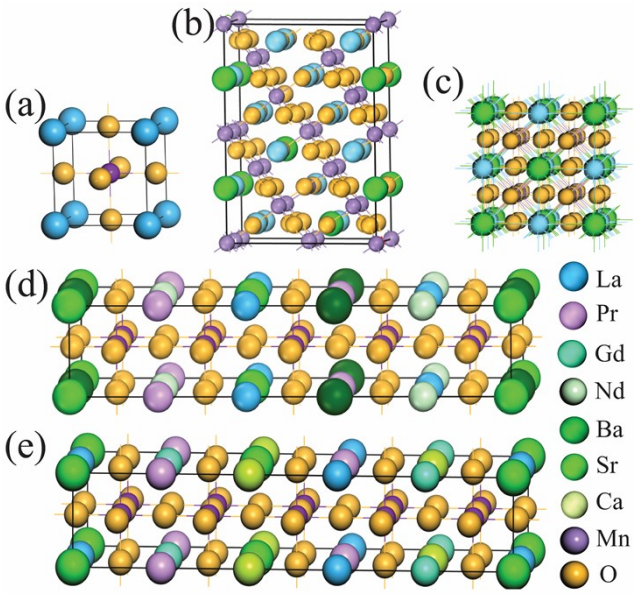


**Fig. S1** Unit cell structure of (a) LMO, (b) LSM20, (c) 2×2×2 supercell of LSM50, 5×2×1 supercells of (d) LSBNP, and (e) LSCGP perovskite oxides.

**Table S2** DFT optimized input crystal structure information of the parent LMO, LSM20, and LSM50 taken from prior experimental studies, LSBNP, and LSCGP.

| **Perovskite Oxide** | **Symmetry (Space group)** | **Lattice parameter (Å)** |
|---|---|---|
| LMO[17] | Cubic ($Pm\bar{3}m$) | a = 3.94 Å |
| LSM20[18] | Trigonal ($R\bar{3}c$) | a = b = 5.595 Å, and c = 13.51 Å |
| LSM50[19] | Cubic ($Pm\bar{3}m$) | a = 3.85 Å |
| LSBNP | Cubic ($Pm\bar{3}m$) | a = 3.90 Å [DFT, This work], 3.878 Å[20] |
| | | $R_{wp}$ $R_p$ $\chi^2$ |

| | | | | |
|---|---|---|---|---|
| | | 8.60[20] | 6.47[20] | 2.77[20] |
| LSCGP | Cubic ($Pm\bar{3}m$) | a = 3.87 Å [This work (Theory)] | | |
| | | a = 3.84 Å [This work (Experiment)] | | |
| | | $R_{wp}$ | $R_p$ | $\chi^2$ |
| | | 6.30 | 6.49 | 2.89 |

## 3. Input parent perovskite oxides for enthalpy of mixing calculations

Crystal structure databases like Materials Project[21] and OQMD[22,23] were used to obtain information on parent perovskite oxides previously synthesized experimentally. The corresponding data is presented in Table S3.

**Table S3** Structural information of parent perovskite oxides from literature.

| **Perovskite Oxide** | **Space group** | **Lattice parameters** | **References** |
|---|---|---|---|
| $LaMnO_3$ | $Pm\bar{3}m$ | a = b = c = 3.94 Å | [Ref.[17]] |
| $PrMnO_3$ | $Pm\bar{3}m$ | a = b = c = 3.89 Å | [Ref.[24]] |
| $NdMnO_3$ | Pnma | a = 5.81 Å, b = 7.61 Å, c = 5.41 Å | [Ref.[25]] |
| $GdMnO_3$ | Pnma | a = 5.33 Å, b = 5.64 Å, c = 7.62 Å | [Ref.[26]] |
| $BaMnO_3$ | P63cm | a = b = 9.84 Å, c = 4.90 Å | [Ref.[27]] |
| $SrMnO_3$ | P63/mmc | a = b = 5.45 Å, c = 9.09 Å | [Ref.[28]] |
| $CaMnO_3$ | Pnma | a = 5.33 Å, b = 5.40 Å, c = 7.57 Å | [Ref.[29]] |

## 4. LSBNP and LSCGP surface slabs terminated along (001) direction

For the Sr-cation segregation study from DFT, A-site cations terminating or Mn terminating slabs are considered in (001) direction. Figure S2 represents the surface slabs of LSBNP and LSCGP along the (001) direction.

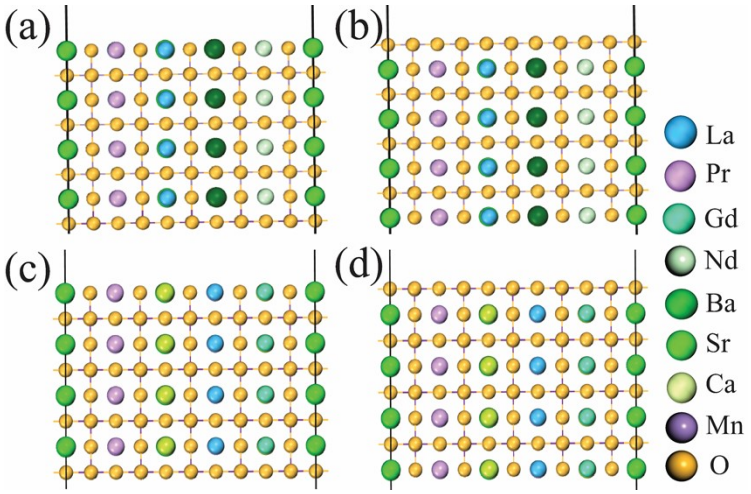


**Fig. S2** (a, c) A-site and (b, d) Mn-site surface terminating slabs of LSBNP and LSCGP, respectively.

## 5. Oxygen vacant structure of LSBNP and LSCGP high entropy perovskite oxides

In order to study oxygen vacancy formation energies, the 5×2×1 supercell of the high entropy structures is considered. Oxygen vacancies are created by removing one oxygen atom from the structure. High entropy structures provide a diverse environment for oxygen vacancy. Hence, all possible oxygen vacancy positions in the AO-plane ($AMnO_3$-based perovskite oxides) are considered, as shown in Figure S3. In the case of the $MnO_2$-plane, the oxygen vacancy position resulting in the lowest energy is presented.

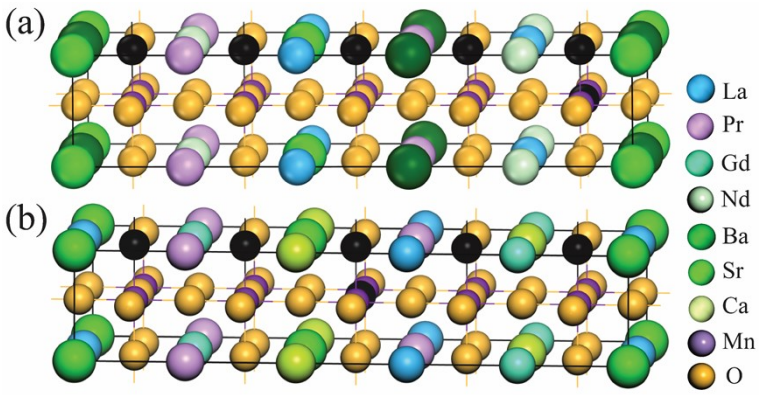


**Fig. S3** Oxygen vacant 5× 2×1 supercell of (a) LSBNP and (b) LSCGP high entropy perovskite oxides, where the black sphere represents the oxygen vacancy site.

## 6. Radial pair distribution function for $Sr^{+2}$-$O^{-2}$ pairs in LSM20, LSM50, LSBNP, and LSCGP surface slabs

The radial pair distribution functions for $Sr^{+2}$-$O^{-2}$ pairs are analyzed from the MD trajectories plotted for Mn-terminated surface slabs of LSM20, LSM50, LSBNP, and LSCGP structures. The diffused RDF plots predict more cation disorder, while the ordered RDF plots predict less cation disorder and hence less Sr-cation segregation towards the surface. Figure S4 (a-d) represents the RDF plots for LSM20, LSM50, LSBNP, and LSCGP structures.

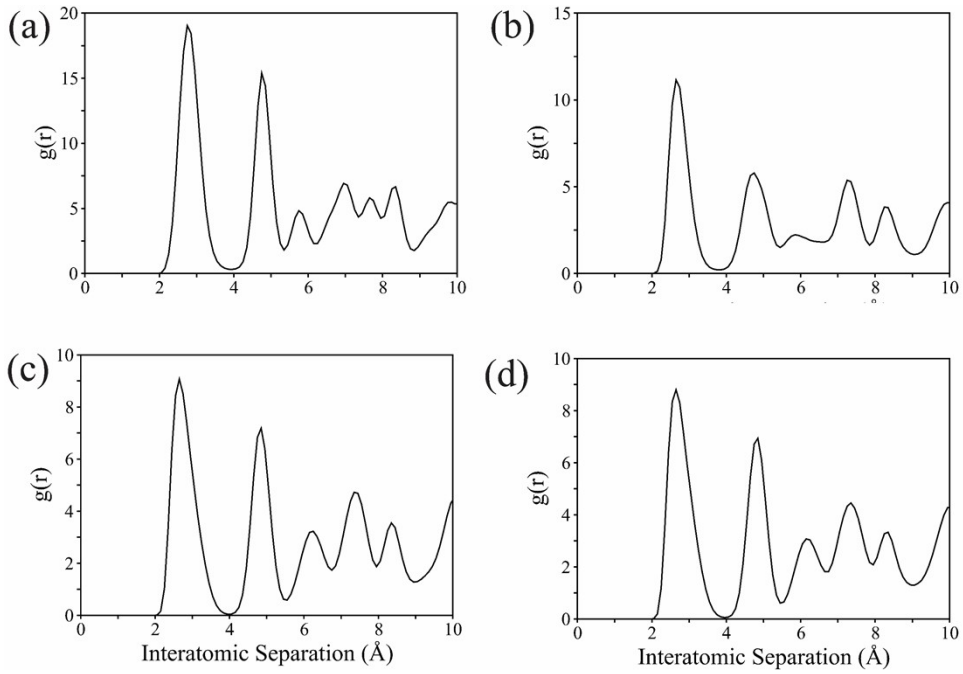


**Fig. S4** Radial pair distribution plot for $Sr^{+2}$-$O^{-2}$ pairs of (a) LSM20, (b) LSM50, (c) LSBNP, and (d) LSCGP.

## 7. Oxygen vacancy formation energy of LSCGP, LSBNP, and reference simple perovskite oxides

Table S4 represents the oxygen vacancy formation energy ($E_{OV}$) for LSCGP, LSBNP, and reference simple perovskite oxides from our DFT simulations and literature.

**Table S4** Oxygen vacancy formation energies (kJ/mol) in various possible sites of LSM20, LSM50, LSBNP, and LSCGP (The A-O-B convention represents A and B ions nearest neighbor ion around the oxygen vacant site).

| Perovskite Oxide | Oxygen Vacancy Formation Energy (kJ/mol) | |
|---|---|---|
| LSCGP | La-O-Pr | 227.41 |
| | Pr-O-Gd | 220.50 |
| | Gd-O-Sr | 223.60 |
| | Sr-O-Ca | 204.48 |
| | Ca-O-La | 214.76 |
| | $MnO_2$ | 166.82 |
| LSBNP | La-O-Pr | 246.65 |
| | Pr-O-Nd | 243.58 |
| | Nd-O-Ba | 244.56 |
| | Ba-O-Sr | 248.30 |
| | Sr-O-La | 247.34 |
| | $MnO_2$ | 212.02 |
| LMO | 302.96 [Ref.[30]]<br>415.85 [Ref.[31]]<br>398.97 [Ref. [32]]<br>409.10 [This work] | |
| LSM20 | 362.78 [This work] | |
| LSM25 | 390.77 [Ref.[31]] | |
| LSM50 | 338.66 [Ref.[31]]<br>302.94 [This work] | |
| $CaMnO_3$ | 193.00 [Ref. [32]] | |
| $BaMnO_3$ | 270.20 [Ref. [32]] | |
| $SrMnO_3$ | 185.25 [Ref. [32]] | |
| $PrMnO_3$ | 309.70 [Ref. [32]] | |
| $GdMnO_3$ | 355.20 [Ref. [32]] | |
| $NdMnO_3$ | 366.60 [Ref. [32]] | |

## 8. MSD vs. time data for LSBNP and LSCGP high entropy perovskite oxides

To calculate oxygen anion diffusivities, MSD vs. time data was extracted from time dynamics of equilibrated structures. For this, MD simulations were performed at 773-1273 K temperatures. Figure S5 shows the MSD vs. time data for LSBNP and LSCGP high-entropy perovskite oxides.

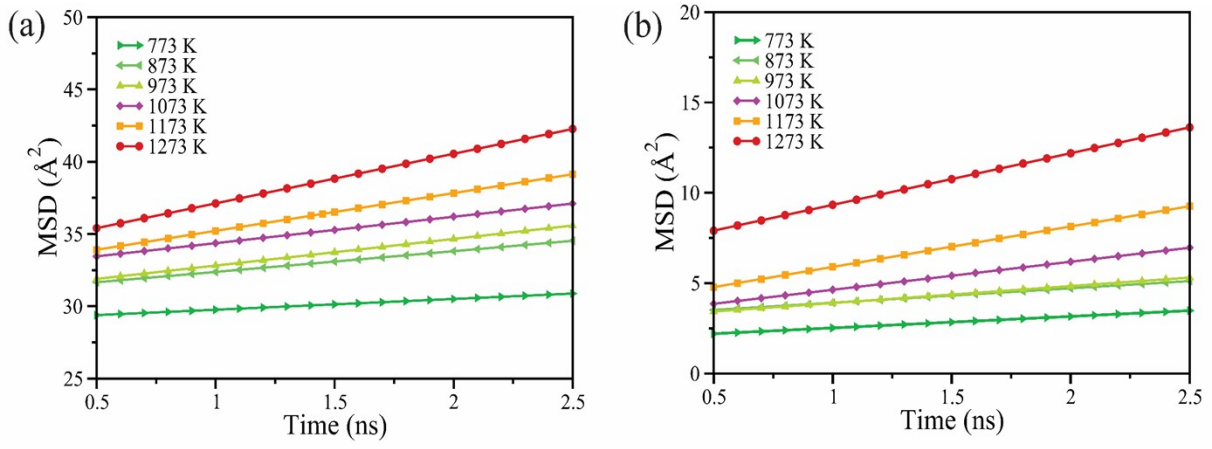


**Fig. S5** MSD vs. time data extracted for (a) LSBNP, (b) LSCGP high entropy perovskite oxide configurations using MD simulations.

## References


1 A. E. Grechanovsky, N. N. Eremin and V. S. Urusov, *Phys. Solid State*, 2013, **55**, 1929–1935, DOI: https://doi.org/10.1134/S1063783413090138.

2 T. S. Bush, J. D. Gale, C. R. A. Catlow, P. D. Battle, M. N. Abser, M. Bellwood, C. M. Buckley, M. C. Holmes and R. W. McCabe, *J. Mater. Chem.*, 1994, **4**, 1765–1765, DOI: https://doi.org/10.1039/JM9940401765.

3 A. Senyshyn, L. Vasylechko, M. Knapp, U. Bismayer, M. Berkowski and A. Matkovskii, *J. Alloys Compd.*, 2004, **382**, 84–91, DOI: https://doi.org/10.1016/j.jallcom.2004.03.146.

4 J. Hermet, G. Geneste and G. Dezanneau, *Appl. Phys. Lett.*, 2010, **97**, 174102, DOI: https://doi.org/10.1063/1.3504250.

5 M. T. Buscaglia, V. Buscaglia, M. Viviani and P. Nanni, *J. Am. Ceram. Soc.*, 2001, **84**, 376–84, DOI: https://doi.org/10.1111/j.1151-2916.2001.tb00665.x.

6 J. R. Tolchard, M. S. Islam and P. R. Slater, *J. Mater. Chem.*, 2003, **13**, 1956–1961, DOI: https://doi.org/10.1039/B302748C.

7 G. V. Lewis and C. R. A Catlow, *J. Phys. C Solid State Phys.*, 1985, **18**, 1149–1161, DOI: https://doi.org/10.1088/0022-3719/18/6/010.

8 W. J. Feng, D. Li, W. J. Ren, Y. B. Li, W. F. Li, J. Li, Y. Q. Zhang and Z. D. Zhang, *Phys.*

*Rev. B*, 2006, **73**, 205105, DOI: https://doi.org/10.1103/PhysRevB.73.205105.

9 M. S. Islam, M. Cherry and C. R. A. Catlow, *J. Solid State Chem.*, 1996, **124**, 230–237, DOI: https://doi.org/10.1006/jssc.1996.0231.

10 M. S. D. Read, M. Saiful Islam, G. W. Watson, F. King and F. E. Hancock, *J. Mater. Chem.*, 2000, **10**, 2298–2305, DOI: https://doi.org/10.1039/B002168G.

11 M. Cherry, M.S. Islam, and C.R.A. Catlow, *J. Solid State Chem.*, 1995, **118**, 125–132, DOI: https://doi.org/10.1006/jssc.1995.1320.

12 A. Van De Walle, P. Tiwary, M. De Jong, D. L. Olmsted, M. Asta, A. Dick, D. Shin, Y. Wang, L. Q. Chen and Z. K. Liu, *Calphad*, 2013, **42**, 13–18, DOI: https://doi.org/10.1016/j.calphad.2013.06.006.

13 A. Van De Wall and M. Asta, *Model. Simul. Mater. Sci. Eng.*, 2002, **10**, 521–538, DOI: https://doi.org/10.1088/0965-0393/10/5/304.

14 A. Van De Walle and G. Ceder, *J. Phase Equilibria*, 2002, **23**, 348–359, DOI: https://doi.org/10.1361/105497102770331596.

15 A. Van De Walle, M. Asta and G. Ceder, *Calphad*, 2002, **26**, 539–553, DOI: https://doi.org/10.1016/S0364-5916(02)80006-2.

16 G. Kresse and J. Furthmüller, *Comput. Mater. Sci.*, 1996, **6**, 15–50, DOI: https://doi.org/10.1016/0927-0256(96)00008-0.

17 M. J. Sayagués, J. M. Córdoba and F. J. Gotor, *J. Solid State Chem.*, 2012, **188**, 11–16, DOI: https://doi.org/10.1016/j.jssc.2012.01.018.

18 S. Zemni, Ja. Dhahri, K. Cherif, Je. Dhahri, M. Oummezzine, M. Ghedira and H. Vincent, Journal of Solid State Chemistry , 2004, **177**, 2387-2393, DOI: https://doi.org/10.1016/j.jssc.2004.03.017.

19 S. Liang, F. Teng, G. Bulgan and Y. Zhu, *J. Phys. Chem. C*, 2007, **111**, 16742–16749, DOI: https://doi.org/10.1021/jp074934m.

20 Y. Shi, N. Ni, Q. Ding and X. Zhao, *J. Mater. Chem. A*, 2022, **10**, 2256–2270, DOI: https://doi.org/10.1039/D1TA07275G.

21 A. Jain, S. P. Ong, G. Hautier, W. Chen, W. D. Richards, S. Dacek, S. Cholia, D. Gunter, D. Skinner, G. Ceder and K. A. Persson, *APL Mater.*, 2013, **1**, 011002, DOI: https://doi.org/10.1063/1.4812323.

22 J. E. Saal, S. Kirklin, M. Aykol, B. Meredig and C. Wolverton, *Jom*, 2013, **65**, 1501–1509, DOI: https://doi.org/10.1007/s11837-013-0755-4.

23 S. Kirklin, J. E. Saal, B. Meredig, A. Thompson, J. W. Doak, M. Aykol, S. Rühl and C. Wolverton, *npj Comput. Mater.*, 2015, 1, 15010, DOI: https://doi.org/10.1038/npjcompumats.2015.10.

24 S. K. Mishra, M. K. Gupta, R. Mittal, A. I. Kolesnikov and S. L. Chaplot, *Phys. Rev. B*, 2016, **93**, 214306, DOI: https://doi.org/10.1103/PhysRevB.93.214306.

25 S. Quezel-Ambrunaz, *Bull. la Société française Minéralogie Cristallogr.*, 1968, **91**, 339–343, DOI: https://doi.org/10.3406/bulmi.1968.6239.

26 A. Modi and N. K. Gaur, *J. Alloys Compd.*, 2015, **644**, 575–581, DOI: https://doi.org/10.1016/j.jallcom.2015.05.022.

27 E. J. Cussen and P. D. Battle, *Chem. Mater.*, 2000, **12**, 831–838, DOI: https://doi.org/10.1021/cm991144j.

28 A. Daoud-Aladine, C. Martin, L. C. Chapon, M. Hervieu, K. S. Knight, M. Brunelli and P. G. Radaelli, *Phys. Rev. B - Condens. Matter Mater. Phys.*, 2007, **75**, 104417, DOI: https://doi.org/10.1103/PhysRevB.75.104417.

29 Q. Zhou and B. J. Kennedy, *J. Phys. Chem. Solids*, 2006, **67**, 1595–1598, DOI: https://doi.org/10.1016/j.jpcs.2006.02.011.

30 E. Olsson, X. Aparicio-Anglès and N. H. De Leeuw, *J. Chem. Phys.*, 2016, **145**, 014703, DOI: https://doi.org/10.1063/1.4954939.

31 N. Lee, Y. Lansac, H. Hwang and Y. H. Jang, *RSC Adv.*, 2015, **5**, 102772–102779, DOI: https://doi.org/10.1039/C5RA21982E.

32 B. Baldassarri, J. He, X. Qian, E. Mastronardo, S. Griesemer, S. M. Haile and C. Wolverton, *Phys. Rev. Mater.*, 2023, **7**, 065403, DOI:

https://doi.org/10.1103/PhysRevMaterials.7.065403.